

A Clinical Feasibility Study on Respiratory Sorted Megavoltage Cone Beam CT

Mingqing Chen, R. Alfredo Siochi

Department of Electrical and Computer Engineering
Department of Radiation Oncology
The University of Iowa

Abstract. In order to improve gated radiotherapy for lung cancer, we explore the use of projection data from localization Mega-voltage cone-beam computed tomography (MVCBCT) scans to reconstruct respiratory correlated images. The position of the ipsilateral hemi-diaphragm apex (IHDA), automatically detected in raw data, is used for projection sorting. Two algorithms, the Feldkamp, Davis and Kress and the simultaneous algebraic reconstruction technique are implemented for incomplete projection reconstruction. The tumor and the IHDA are manually identified on full exhale and full inhale phases of MVCBCT images. 16 MVCBCT scans and 2 planning CT scans of a non-small cell lung cancer patient are analyzed. Results show that it is feasible to use sorted projection reconstruction to determine relationship between the tumor and the diaphragm motion and observe tumor volume change due to effect of radiotherapy.

Keywords: diaphragm, respiratory motion, cone beam CT, reconstruction

1 Introduction

Respiratory motion is a major concern in radiotherapy for lung tumors. In our clinic, a strain gauge system is used during the planning CT scan to record the relative respiratory phase and create 4DCT images that allow us to determine the phases to be used for treatment. The strain gauge system is considered an external surrogate of tumor motion and provides respiratory gating signals to turn the treatment beam on or off. However, tumor motion may vary from one fraction to the next, and may be different from the motion at the time of the 4DCT. Because this variation can cause tumor underdose or overexpose normal tissue, the strain gauge should be calibrated to tumor motion.

Mega voltage cone beam CT (MVCBCT) is a promising technique for daily imaging of patients [20, 22]. It only provides one static image reconstructed from all the raw images projected from different gantry angles. For static organs, inter-fractional changes are observable. But intra-fractional changes such as tumor and diaphragm motion are averaged over all projections, which makes it difficult to observe the tumor size and shape before each treatment fraction. Utilizing

MVCBCT projection images is a promising solution. Reitz et al. [23] projected 3D tumor volume onto projections to verify the tumor position prior to radiotherapy. Siochi developed a semi-automatic method to determine respiratory-like motion of a tungsten pin on projection images with minimal manual input [25]. Unlike these objects with clearly defined edges, the tumor boundary is not visible in many views. Methods that work well with fluoroscopic images [6,18,28,29] may not be suitable for the application of MVCBCT projection images. Alternatively, the diaphragm has sudden changes in intensity in most views and its motion is a more accurate internal surrogate for tumor motion [4,27]. The strain gauge could be calibrated to tumor motion indirectly using the diaphragm. We previously developed a dynamic Hough transform (DHT) method based on Lappas' work [15,16]. It was able to detect the ipsilateral hemi-diaphragm apex (IHDA) positions in all MVCBCT projection views within a minute [5] (The IHDA is the most superior point in all projection views of one hemi-diaphragm). Compared to the method introduced by Sonke et al. [26], which projects the diaphragm in 2D CBCT projection images to 1D to extract relative respiratory phase, our previous method detects the actual 3D anatomical position of the IHDA. The algorithm is not robust in a few lateral views when both hemi-diaphragms are overlapping each other (figure 3a). Manual tuning of DHT parameters may correct the ambiguous recognition. It is also required to establish the relationship between diaphragm motion and tumor motion.

In this work, we further investigated the feasibility of identifying the tumor in MVCBCT images reconstructed from respiratory phase sorted data. First, a more robust method for IHDA detection especially for problems in lateral views is presented. Secondly, projection images are sorted to full inhale (FI) and full exhale (FE) phases based on the IHDA position. Volumetric 3D images are reconstructed from sorted projections. The tumor boundary and the IHDA position in each 3D image set are manually identified. Tumor size, tumor centroid and the diaphragm to tumor motion ratio (DTMR) are quantified.

2 Materials and Methods

2.1 MVCBCT Data

MVCBCT projection data are acquired as the gantry rotates. The standard protocol for rotation is 200 degrees from -90° to 110° , with one projection per degree. The images are acquired with an amorphous Si flat panel electronic portal imaging device (EPID) with a detector pixel size of $0.4 \times 0.4\text{mm}^2$. It has a source to axis distance (SAD) of 100 cm, a source to imager distance (SID) of 145 cm, and an imaging field of view (FOV) of $27.4 \times 27.4\text{cm}^2$. The EPID has a resolution of 1024×1024 , with a pixel spacing of 0.4mm . MVCBCT raw data are taken from one NSCLC patient who was treated with five fractions each week for almost 8 weeks. The imaging protocol used a 10MU exposure, with an acquisition time of 55s. MVCBCT scans performed on each Thursday and Friday and two planning CTs are studied. The first planning CT was taken six days

before the first treatment day (a Thursday) while the second one was taken on the Thursday of the 4th week.

2.2 IHDA Detection in Projected Images

The Hough transform (HT) is a robust object detection technique specified for prior known parametric shapes [1, 7, 13]. It is based on global evidence accumulation in shape parameter space. Over the years, different variations of HT for motion detection in image sequences were developed, including global optimization based approaches such as velocity HT [21] and dynamic HT (DHT) [15, 16], and tracking based approaches [11, 12, 19].

Our previous method for IHDA detection can be found in [5], which employs a Hough transformation for all ROIs of the projection images. The hemidiaphragm in MCBCT projections is modeled by two parabolas connected at their common vertex (x_0, y_0) , with focal lengths of $4a_1$ and $4a_2$, with representation as:

$$\begin{aligned} f(x) &= a_1(x - x_0)^2 + y_0, \text{ if } x \leq x_0 \\ &= a_2(x - x_0)^2 + y_0, \text{ if } x > x_0 \end{aligned} \quad (1)$$

A five dimensional (5D) Hough accumulator array $I(x_0, y_0, a_1, a_2, t)$ is built with each cell representing a two-parabola contour, where t is the index of projection image. It is then reduced into the 3D parameter space of $I(x_0, y_0, t)$ by maximal intensity projection (MIP) for computation efficiency, with two associated arrays $a_1(x_0, y_0, t)$ and $a_2(x_0, y_0, t)$ recording the corresponding a_1 and a_2 . The optimal motion trajectory of the IHDA over all images is detected by dynamic programming.

The method presented here employs a frame-by-frame point tracking technique in Hough arrays. The program starts to track through an entire MCBCT raw image sequence from four frames with the IHDA identified by the user. The IHDA position is then determined frame by frame iteratively. In each iteration, as the IHDA position of the current frame is determined, a joint probability function is evaluated for every local maxima of Hough space in the next frame. The maxima with the largest probability is picked. The joint probability function is:

$$\begin{aligned} f(x_0^{t+1}, y_0^{t+1}, a_1^{t+1}, a_2^{t+1}) &= f_x(x_0^{t+1}|x_0^t)f_y(y_0^{t+1}|y_0^t) \\ &\quad f_a(a_1^{t+1}|a_1^t)f_a(a_2^{t+1}|a_2^t)f_{cor}(x_0^{t+1}, y_0^{t+1}|x_0^t, y_0^t) \end{aligned} \quad (2)$$

Where superscripts t and $t + 1$ represent the current and next frame, respectively. The joint probability function has five components, each measuring the conditional probability of parameters in the next frame using the current frame as its input. Functions f_x , f_y , f_a measure probability based on parabola

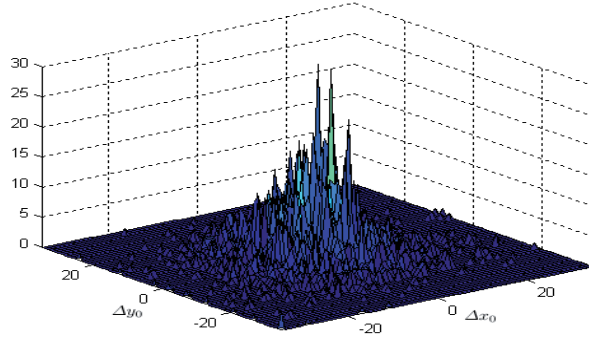


Fig. 1: Distribution of IHDA positions in 21 MVCBCT projection sets represented by Δx_0 and Δy_0

parameters x_0, y_0, a_1 and a_2 respectively. f_{cor} determines the probability of a local maxima candidate in frame $t+1$ based on the normalized cross correlation (NCC) [3]. The NCC is computed between two image patches in Hough space, one of which consists of the neighboring pixels of the local maxima candidate in frame $t+1$, while the other is the group of neighboring pixels of the IHDA in frame t .

The conditional probability of the five components are assumed to be Gaussian distributions. The mean values for functions f_x , f_y , f_a are the parabola parameters of the current frame and for f_{cor} , it is 1.0, which represents two identical images.

$$f_x(x_0^{t+1}, x_0^t) = k_x e^{-\frac{(x_0^{t+1} - x_0^t)^2}{2\sigma_x^2}} \quad (3)$$

$$f_y(y_0^{t+1}, y_0^t) = k_y e^{-\frac{(y_0^{t+1} - y_0^t)^2}{2\sigma_y^2}} \quad (4)$$

$$f_a(a^{t+1}, a^t) = k_a e^{-\frac{(a^{t+1} - a^t)^2}{2\sigma_a^2}} \quad (5)$$

$$f_{cor} = k_{cor} e^{-\frac{(NCC(x_0^{t+1}, y_0^{t+1}, x_0^t, y_0^t) - 1)^2}{2\sigma_{cor}^2}} \quad (6)$$

The Gaussian window σ is derived from a statistical analysis of the manual IHDA identification results on 40 MVCBCT scans from 6 patients. Figure 1 shows the distribution of IHDA displacements, which is similar to a 2D Gaussian distribution.

The IHDA positions in 2D projections are converted to the IHDA positions in the patient coordinate system based on an interpolated ray tracing method [25]. The IHDA position in the patient is used for respiratory sorted reconstruction.

2.3 Respiratory Correlated MVCBCT

Current MVCBCT imaging uses all the projections to reconstruct a static image. By selecting projections belonging to the same respiratory phase, it is possible to reconstruct MVCBCT images of moving tumors with multiple phases. In this study the FE and FI phases are reconstructed for each MVCBCT scan. The superior-inferior position of the IHDA, provided by the previous step, is scaled from 0 to 100 to represent normalized respiratory phases. The ideal phase bin for the FE phase should be 0 to *phasewindow*, and $(100 - \text{phasewindow})$ to 100 for the FI phase. But for real respiratory traces, especially for irregular breathing, inclusion of 0 or 100 will only encompass a small amount of projections. Both factors should be considered for proper phase window and level values. An exhaustive search strategy is applied to find these values. For the FI phase, it aims to find a phase window and level that maximize the averaged respiratory amplitude of projections within the phase window. For the FE phase, the same procedure is used for minimization of the amplitude.

The default CBCT reconstruction algorithm by Feldkamp, Davis, and Kress (FDK) [8], is fast and produces good images, but an inadequate number of projections results in strong aliasing artifacts. Algorithms derived from Algebraic reconstruction techniques (ART) [10] are more robust for incomplete projections but require much more computation time due to iterative re-projection and back-projection [14]. Hardware acceleration based on graphic cards made it feasible to accomplish cone beam ART reconstruction within a clinical time limit [24]. In this work, both methods are investigated to evaluate the feasibility of tumor contouring without considering reconstruction speed. MVCBCT projection matrices, which were derived during MVCBCT geometric calibration [20], are used for voxel-driven projection computations in FDK and ray-driven models in ART [9]. A Bessel-Kraiser filter [17] is used as the interpolation kernel for ART, since it has less aliasing artifacts than bilinear or Gaussian kernels for ray-driven back-projection.

The IHDA position and tumor boundary in both FE and FI images are identified by a researcher without prior knowledge of the patient using the Pinnacle treatment planning software. The volume and centroid of the tumor and the DTMR are then calculated. These parameters are also quantified on the planning CT for comparison. Figure 4 shows one example of manual contouring of the tumor using Pinnacle.

3 Results and Discussions

3.1 IHDA Detection

For each MVCBCT scan, automatic IHDA detection is compared to the independent manual identification in the raw data, which is considered as ground truth. Root mean square (RMS) errors are calculated and compared with those of the DHT method on 19 images from 6 patients. In figure 2, DHT has a large

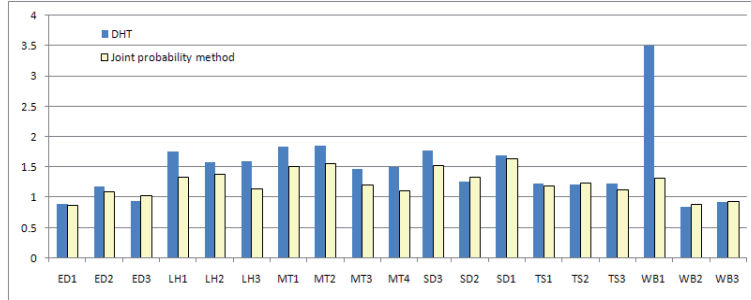


Fig. 2: Comparison between DHT and new point tracking method on RMS error (in mm) in 19 MVCBCT scans.

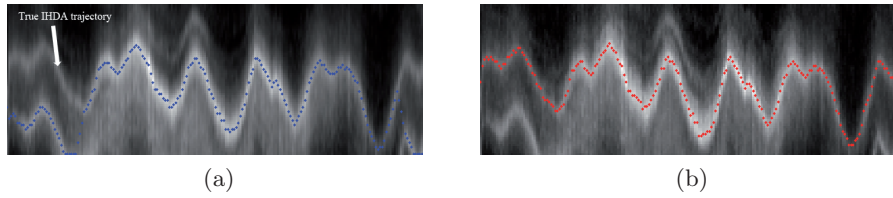


Fig. 3: 2D representation of Hough accumulator array. Each column represents a 1D Hough image of a projection frame. One example of IHDA trajectory detected by (a) DHT with inter-column constraint 5; (b) The new point tracking method.

error for one image due to the erroneous detection of the contra-lateral hemidiaphragm (CHD) in a number of frames. The new method corrects this problem and reduces RMS errors. Of the 19 images, 14 have improved accuracy due to reduced cases of CHD detection and improved accuracy in IHDA localization. For the other 5 images, both of the methods are accurate enough and the difference in the RMS is small, and can be considered a statistical fluctuation. Overall, the new method presented in this work achieves a mean RMS error of 1.228mm with a standard deviation of 0.220mm , compared to the DHT result of $1.341\text{mm} \pm 0.640\text{mm}$.

For the DHT method, using a global optimization strategy seems to be an advantage over the new method. It aims to maximize an energy function composed of Hough values and motion penalties on motion trajectories by using a dynamic programming (DP) technique. However, the existence of the CHD in some lateral views makes the global optimization strategy error-prone. Although the hard inter-frame constraint used in DP restricts the sudden jump of the IHDA position from one hemi-diaphragm to the other, the optimization strategy tends to find stronger features in Hough space (Figure 3a). In our experiment, finding the most probable Hough peak with a given variation in position, parabola curvature and image intensity in a neighborhood continuously over the image sequence is more likely to track the correct hemi-diaphragm (figure 3b).

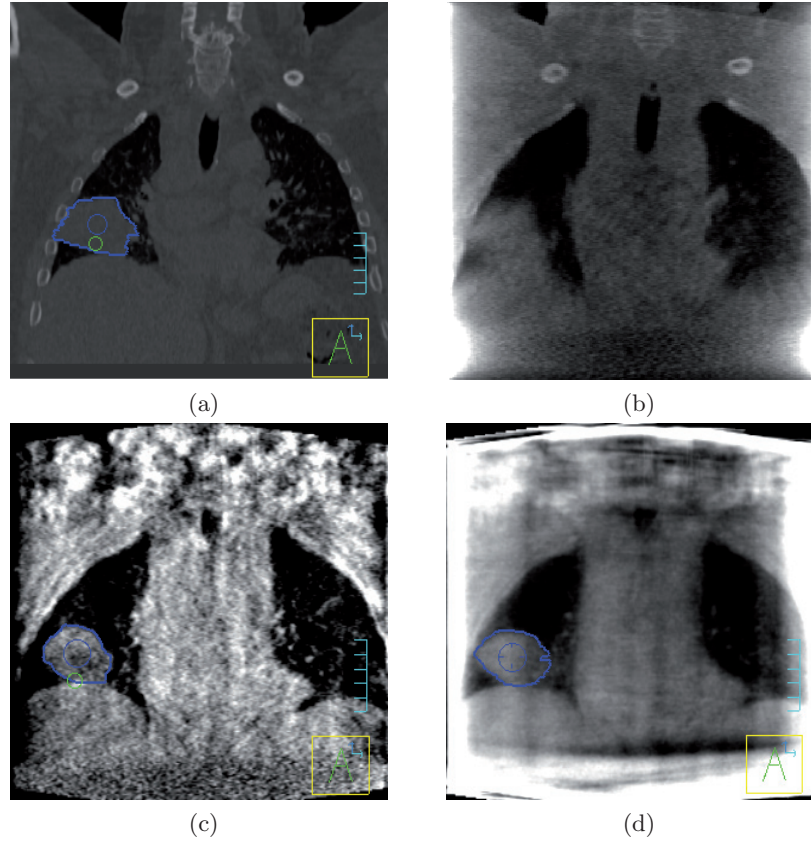


Fig. 4: Image reconstruction example slice in coronal view: (a) FE phase of planning CT; (b) FDK-MVCBCT reconstructed from all the projections; (c) FE phase of FDK-MVCBCT; (d) FE phase of ART-MVCBCT. Tumor contour is displayed as blue

3.2 Respiratory Correlated Reconstruction

Figure 4a shows one coronal slice of a 4D planning CT. The MVCBCT has a much lower contrast to noise ratio (CNR). In figure 4b a MVCBCT image reconstructed using all the projection data is shown. Static tissues such as shoulders are visible, but objects in motion, such as ribs, hemi-diaphragms and the tumor are very blurred. In the example image of the respiratory sorted reconstruction, the tumor boundary and diaphragm are better defined, regardless of the reconstruction method: FDK (figure 4c) or ART (figure 4d). Reconstruction artifacts existed in both FDK-MVCBCT and ART-MVCBCT, further degrading the image quality. Both FDK and ART have truncation artifacts at the border of the imaging FOV. The intensities of organs outside the FOV contribute to the

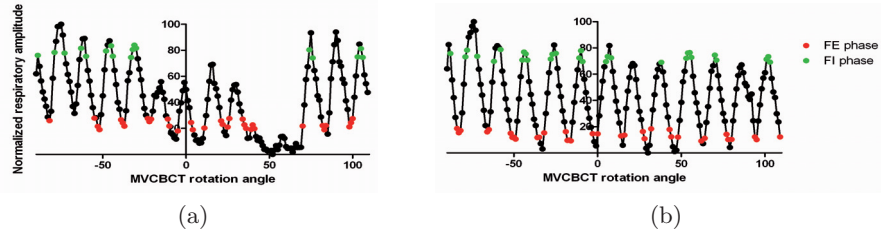


Fig. 5: Normalized respiratory phase for (a) irregular breath (b) regular breath

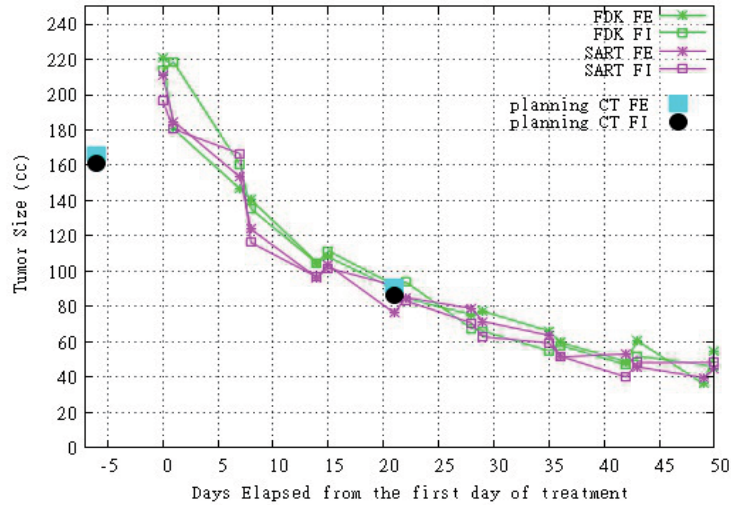


Fig. 6: Tumor volume plotted against elapsed days from first fraction

voxel at the FOV border during back-projection. For FDK, the streak artifact is observable, which is due to incomplete projections.

The patient received audio-coaching during the treatment in order to encourage regular breathing. While this makes the gated RT treatment more reliable, it can also help improve the reconstruction of limited projection data by avoiding large gaps of missing projections. However there are some exceptions when the patient is unable to maintain the regularity during the scan. In our study, the IHDA respiratory phase in one of 16 MVBCT images shows a very irregular pattern (figure 5a), where the respiratory amplitudes for some maxima are much smaller than those of the other maxima. The exhaustive search strategy had a hard time for this image, since no projections are within the FI phase window from frame 60 to 160 (figure 5a). The image reconstructed in this projection set is severely degraded, making it impossible to contour the tumor correctly. For reference, figure 5b shows a regular breathing pattern.

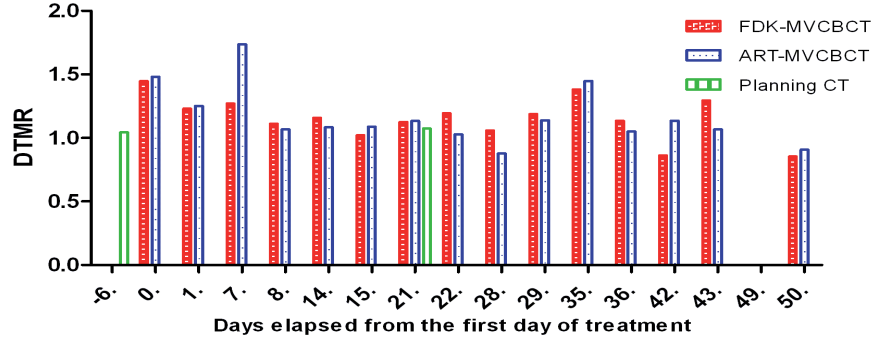


Fig. 7: DTMR value for 15 MVCBCT and 2 planning CT (MVCBCT with irregular breathing is excluded)

The radiation effect on tumor volume over the course of radiotherapy is plotted in figure 6. Images reconstructed by FDK and ART are both studied. The effect of radiotherapy shows an exponential pattern of volume shrinkage. The average discrepancy in tumor volume between FDK and ART methods is 9.38%, with a standard deviation of 7.2%. The discrepancy between the two methods may be due to human subjective error and improper setting of display window and level, which is shown to affect the object size measurement [2]. Although small errors existed between FDK and ART in size measurement, both methods agree well for the purpose of monitoring the trend of tumor change. Tumor volumes derived from two 4D planning CT scans are also shown in the graph, which can be considered as a gold standard. For the planning CT taken 6 days before the start of radiotherapy treatments, the tumor size is much smaller than the tumor size in both FDK-MVCBCT and ART-MVCBCT images taken minutes before the first radiation treatment. This may be due to tumor growth during the 6 day interim between imaging and treatment, since there is no radiation given during the 6 day interim and the tumor was particularly aggressive. The tumor size contoured in the second planning CT agrees well with the MVCBCT taken on the same day.

DTMR values are plotted in figure 7, which is computed from the IHDA motion and tumor motion displayed in figure 8. The measured motion is generally consistent between FDK-MVCBCT and ART-MVCBCT. The measured IHDA motion ranges from 0.78cm to 2.17cm, with an average and standard deviation of the difference between FDK and SART methods of $0.058cm \pm 0.052cm$. The tumor motion ranges from 0.8cm to 1.82cm, with a deviation between the two methods of $0.131cm \pm 0.112cm$. Comparing tumor and IHDA motion to the slice thickness in the superior-inferior direction, which is 1.071mm and 3.0mm for the MVCBCT and 4DCT respectively, variation by one voxel in the IHDA identification may induce a 10% DTMR change. This error is consistent with the average

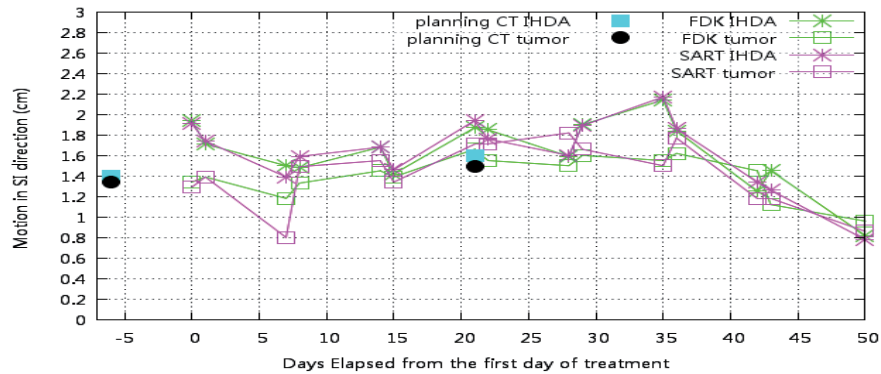


Fig. 8: Motion of IHDA and tumor centroid for 15 MVCBCT and 2 planning CT (MVCBCT with irregular breathing is excluded)

difference between FDK and ART measurements. There are a few cases with a significant exception such as the one on day 7. The motion of both the IHDA and the tumor centroid in this scan is relatively small. The division between the two measured motions to compute the DTMR further increases the inaccuracy, which is part of the reason for the larger error. DTMR from the planning 4DCT taken 6 days before the first treatment day is much smaller than that of the MVCBCT, possibly due to discrepancies in tumor volume and/or natural variations in breathing patterns from one day to the next. For the planning 4D CT taken on the 4th week, the DTMR is close to that of the MVCBCT. Typically most images have a DTMR larger than 1, which is consistent with lung expansion during inhale. For the few cases where DTMR is smaller than 1, they may be due to manual identification and contouring errors, but it is also possible that the patient was breathing more with their chest than with their diaphragm.

In this study we have verified the feasibility of assessing tumor response based on respiratory sorted MVCBCT derived tumor volumes. Parameters measured for the tumor contour and the IHDA in MVCBCT images are close to those of the planning CT and are in a reasonable range, except for a few cases in the first week of the MVCBCT, probably due to the time delay between 4DCT imaging and the first treatment fraction. The comparison of the DTMR for planning CT data and MVCBCT data also shows that it is feasible to use limited projection reconstruction to determine the tumor and diaphragm motion relationship. Although the result is only based on one patient and it is hard to draw a conclusion about lung volume measurement accuracy, it shows the feasibility of observing trends in tumor size changes and measuring the DTMR to establish a relationship between tumor and diaphragm motion.

Reconstruction artifacts induced by incomplete projections and truncations are the main reasons that affect tumor contour accuracy. The accuracy of using respiratory sorted MVCBCT reconstruction to measure object size and motion

still needs to be assessed. It will be very helpful to image an object with prior knowledge about its density, shape and size, in order to quantify the reconstruction error. Our future study will focus on phantom design and quantification of the reconstruction accuracy.

References

1. Ballard, D.: Generalizing the hough transform to detect arbitrary shapes. *Pattern recognition* 13(2), 111–122 (1981)
2. Baxter, B., J., S.: Factors affecting the measurement of size and ct number in computed tomography. *Investigative Radiology* 16(4), 337–41 (1981)
3. Briechle, K., Hanebeck, U.: Template matching using fast normalized cross correlation. vol. 4387, pp. 95–102 (2001), proceedings of SPIE
4. Cervino, L.I., Chao, A.K., Sandhu, A., Jiang, S.B.: The diaphragm as an anatomic surrogate for lung tumor motion. *Phys Med Biol* 54(11), 3529–41 (2009)
5. Chen, M., Siochi, R.: Diaphragm motion quantification in megavoltage cone-beam ct projection images. *Medical Physics* 37, 2312–20 (2010)
6. Cui, Y., Dy, J., Sharp, G., Alexander, B., Jiang, S.: Multiple template-based fluoroscopic tracking of lung tumor mass without implanted fiducial markers. *Physics in medicine and biology* 52, 6229–6242 (2007)
7. Duda, R., Hart, P.: Use of the hough transformation to detect lines and curves in pictures (1972)
8. Feldkamp, L., Davis, L., Kress, J.: Practical cone-beam algorithm. *Journal of the Optical Society of America A* 1(6), 612–619 (1984)
9. Galigekere, R., Wiesent, K., Holdsworth, D.: Cone-beam reprojection using projection-matrices. *IEEE transactions on medical imaging* 22(10), 1202–1214 (2003)
10. Gordon, R., Bender, R., Herman, G.: Algebraic reconstruction techniques (art) for three-dimensional electron microscopy and x-ray photography*. 1. *Journal of theoretical Biology* 29(3), 471–481 (1970)
11. Greenspan, M., Shang, L., Jasiobedzki, P.: Efficient tracking with the bounded hough transform. vol. 1. IEEE Computer Society; 1999 (2004)
12. Hills, M., Pridmore, T., Mills, S.: Object tracking through a hough space. pp. 53–56. London; Institution of Electrical Engineers; 1999
13. Hough, P.: Method and means for recognizing complex patterns (1962)
14. Jouvelot, P., Gifford, D.: Algebraic reconstruction of types and effects. p. 310. ACM (1991), proceedings of the 18th ACM SIGPLAN-SIGACT symposium on Principles of programming languages
15. Lappas, P., Carter, J., Damper, R.: Robust evidence-based object tracking. *Pattern Recognition Letters* 23(1-3), 253–260 (2002)
16. Lappas, P., Damper, R., Carter, J.: Object tracking by energy maximization. *Soft Computing-A Fusion of Foundations, Methodologies and Applications* 10(1), 20–26 (2006)
17. Lewitt, R.: Multidimensional digital image representations using generalized kaiser-bessel window functions. *Journal of the Optical Society of America A* 7(10), 1834–1846 (1990)
18. Lin, T., Cervino, L.I., Tang, X., Vasconcelos, N., Jiang, S.B.: Fluoroscopic tumor tracking for image-guided lung cancer radiotherapy. *Phys Med Biol* 54(4), 981–92 (2009)

19. Mills, S., Pridmore, T., Hills, M.: Tracking in a hough space with the extended kalman filter. p. 173?82. Citeseer (2003), british Machine Vision Conference
20. Morin, O., Gillis, A., Chen, J., Aubin, M., Bucci, M., Roach III, M., Pouliot, J.: Megavoltage cone-beam ct: System description and clinical applications. *Medical Dosimetry* 31(1), 51–61 (2006)
21. Nash, J., Carter, J., Nixon, M.: Dynamic feature extraction via the velocity hough transform. *Pattern Recognition Letters* 18(10), 1035–1047 (1997)
22. Pouliot, J., Bani-Hashemi, A.: Low-dose megavoltage cone-beam ct for radiation therapy. *International Journal of Radiation Oncology* Biology* Physics* 61(2), 552–560 (2005)
23. Reitz, B., Gayou, O., Parda, D., Miften, M.: Monitoring tumor motion with on-line mega-voltage cone-beam computed tomography imaging in a cine mode. *Physics in Medicine and Biology* 53(4), 823–836 (2008)
24. Schiwietz, T., Bose, S., Maltz, J., Westermann, R.: A fast and high-quality cone beam reconstruction pipeline using the gpu. *Medical Imaging 2007: Physics of Medical Imaging* 6510 (2007)
25. Siochi, R.: Deriving motion from megavoltage localization cone beam computed tomography scans. *Physics in Medicine and Biology* 54, 4195 (2009)
26. Sonke, J., Zijp, L., Remeijer, P., van Herk, M.: Respiratory correlated cone beam ct. *Medical Physics* 32(4), 1176–86 (2005)
27. Vedam, S., Kini, V., Keall, P., Ramakrishnan, V., Mostafavi, H., Mohan, R.: Quantifying the predictability of diaphragm motion during respiration with a noninvasive external marker. *Medical Physics* 30, 505 (2003)
28. Xu, Q., Hamilton, R.J., Schowengerdt, R.A., Alexander, B., Jiang, S.B.: Lung tumor tracking in fluoroscopic video based on optical flow. *Med Phys* 35(12), 5351–9 (2008)
29. Xu, Q., Hamilton, R., Schowengerdt, R., Jiang, S.: A deformable lung tumor tracking method in fluoroscopic video using active shape models: a feasibility study. *Physics in Medicine and Biology* 52(17), 5277–5294 (2007)